SSRG International Journal of Mechanical Engineering
ISSN: 2348-8360/ https://doi.org/10.14445/23488360/IJME-V12I12P102

Volume 12 Issue 12, 10-18, December 2025

Original Article

Structural and Fluid Dynamics Assessment of Vortex Wind Turbines in Resonant Conditions

Dulce María Graciano[1], Juan Carlos García[1*], José Alfredo Rodríguez[1], Rogelio Martínez-Oropeza[1], Eder Uriel Martínez-Sandoval[1], Christian Marisol Clemente[2], Ángel Sánchez Cruz[3]

[1]*Centro de Investigación en Ingeniería y Ciencias Aplicadas (CIICAp), Universidad Autónoma del Estado de Morelos, Morelos, México.*
[2]*Departamento de ingeniería Industrial y Manufactura, Universidad Autónoma de Ciudad Juárez, Chihuahua, México.*
[3]*Instituto de Energías Renovables, Universidad Nacional Autónoma de México, Morelos, México.*

[*]*Corresponding Author : jcgarcia@uaem.mx*

Received: 04 October 2025 Revised: 05 November 2025 Accepted: 07 December 2025 Published: 27 December 2025

Abstract *- A vortex wind turbine operates without blades, harvesting wind kinetic energy through oscillations, based on the fluid-structure interaction of Vortex-Induced Vibrations (VIV). This research evaluates a vortex wind turbine under resonance conditions using numerical techniques, including Finite Element Method (FEM) and Computational Fluid Dynamics (CFD). The effects of the vortex wake on structural displacements and the useful life of Vortex Wind Turbines (VWT) were analyzed. The results show that the turbine could operate under resonance conditions without risk of mechanical fatigue failure, providing continuous operation.*

Keywords *- Bladeless, Fatigue life, Vortex Induced Vibrations, Vortex Wind Turbine.*

1. Introduction

Today, there is a growing demand for sustainable and environmentally friendly electricity generation technologies. One of the most widely available renewable energies is wind. This energy is conventionally harnessed using horizontal and vertical-axis turbines. However, these technologies have some drawbacks, such as wear and tear on mechanical components, ambient noise, and, in some configurations, the need to align them with the direction of flow.

Considering these drawbacks, the Vortex Wind Turbine (VWT) was designed by Yañez as an alternative technology. This is a simulation without a bladeless to promote the Wind-Induced Resonance (WIR) through fluid-structure interaction. The VWT is a bluff-shaped structure with a flexible base and circular transversal shape. The WIR requires an alternative vortex shedding and a vortex frequency that approaches the natural frequency of the wind turbine [1].

Vortex formation occurs due to boundary layer separation, which arises when a fluid flows past a body and encounters an adverse pressure gradient. This gradient causes the boundary layer, a thin region where viscous forces dominate, to detach from the surface. Once separated, the flow generates alternating regions of high and low pressure behind the body, leading to periodic vortex shedding. This vortex shedding wake, called Von Kármán vortex street, is influenced by the Reynolds number (*Re*), which governs the flow characteristics and stability [2-13].

The vortex shedding frequency is influenced by the Strouhal number (*St*), which relates this frequency to the flow velocity and the characteristic length of the body, have tried to characterize the vortex shedding frequency through a relation between the *Re* – *St* number, although there is a trend in the behavior of the *Re* – *St* relation, the Strouhal values for certain Reynolds differ in most of the studies, so that the adjustment equations usually vary between authors [14-19]. Furthermore, Derakhshandeh reports that the relationship varies with the analyzed geometry [20]. For Re between 300 and $3x10^5$ the $St \cong 0.2$ [21]. However, the experimental *Re-St* curve of a circular cylinder reported by Goldstein shows that if $100 < Re < 1x10^3$ the curve has an upward behavior, but for Re 10^3 to $10^{4.5}$ the curve has a slight decay, to later behave hastily again [22]. A similar phenomenon occurs in the experimental curve of a sphere reported by Sakamoto, where the curve descends when *Re* approaches $3 x10^3$ and begins to rise again when *Re* = $6 x10^3$ [23]. The *Re-St* behavior arises from the varying characteristics of flow regimes and vortex shedding patterns. Differences in geometry, flow conditions, and surface roughness further contribute to specific deviations in the Re-St relationship. The geometric characteristics of the vortex wind turbine determine the WIR phenomenon. The numerical results of the dynamic modeling of VWT reported by

Chizfahm show that the longitudinal shape of the VWT has a role in its performance [24]. VWTs with a conical longitudinal shape work better at high wind speeds, while VWTs with a cylindrical longitudinal shape work better at low wind speeds. The conical shape shows a pattern of vortex shedding frequency fit to the velocity profile caused by the atmospheric boundary layer [25-28].

The VWT seeks to reach a permanent resonance state, to harness a greater amount of energy from the VIV phenomenon, because this state causes the maximum amplitude of vibration. However, a permanent resonance state can induce mechanical fatigue, since repeated stress cycles can cause the collapse and fracture of the structure. The number necessary to generate the fracture depends on various factors, such as the amplitude of the applied load, the material, the presence of small cracks, micro-cracks, and irregularities in the structure, among others [29]. Therefore, the vortex wind turbine can reach failure due to mechanical fatigue. The number necessary to generate the fracture depends on various factors, such as the amplitude of the applied load, material, small cracks, micro-cracks, and irregularities in the structure, among others [30].

Therefore, a mechanical fatigue analysis is necessary to estimate the VWT fatigue life. An experimental mechanical fatigue study in a vortex wind turbine has not been reported yet. But Yañez carried out an analytical calculation where he considers that the vortex wind turbine has a carbon fiber rod subjected to cyclical dynamic load bending, with a maximum angle =2.7°; with an uninterrupted operating frequency = 5 Hz, and estimates a useful lifetime=19.83 years for this [30].

On the other hand, Breen et al. carried out an analytical study to optimize the VWT geometry to generate greater power, maintain structural integrity, and identify configurations capable of reaching up to 460 W without damage to the structure [31].

This study examines the vortex wind turbine behaviour under resonance conditions, using numerical modeling with CFD-FEM to simulate in detail the physical phenomenon of fluid-structure interaction. The geometry studied is based on the scale semi-rigid model proposed by Cajas [25]. The Reynolds (*Re*) and Strouhal (*St*) numbers curve for $2.65x10^2<Re<6.64x10^3$ is reported. The VWT oscillation displacements due to wind-induced resonance and the mechanical fatigue analysis, for this state, are reported.

2. Governing Parameters

Wind-induced resonance is a Fluid-Structure Interaction (FSI) phenomenon, where a structure subjected to aerodynamic forces exerted by air undergoes deformation. This deformation, in turn, affects the flow field, adding complexity to the phenomenon. This study primarily focuses on the structural response, so only the structural changes have been considered, while changes in the flow field have been disregarded. The key parameters governing FSI are the Reynolds and Strouhal numbers, which influence the vortex shedding frequency, the strength of the vortices, and the pressure. Together, these factors affect the dynamics of the fluid-structure interaction. The Re number is a relation between the inertial and viscous forces of a fluid, as in Equation (1).

$$Re = \frac{ud}{v} \tag{1}$$

Where u is the flow velocity, d is the diameter of the VWT, and v is the kinematic viscosity of the fluid. Moreover, the St establishes a relation between the detachment vortex frequency, air stream velocity, and structure geometry characteristics. The *St* value depends on *Re* and, conventionally, is defined as follows:

$$St = \frac{fd}{u} \tag{2}$$

Where f is the detachment vortex frequency.

3. Methodology

This investigation focuses on one-way fluid-structure interaction; Figure 1 shows the numerical analyses workflow. First, the structure's natural frequency is determined using modal analysis, and then the wind velocity that induces resonance in the structure is identified using 2D CFD simulations. This velocity is used as a boundary condition in the 3D CFD simulations to obtain the pressure profiles on the structure under resonant conditions. These profiles serve as boundary conditions in the harmonic analysis to obtain the displacements of the structure at resonance. Finally, the displacements obtained are used as operation criteria in the mechanical fatigue analysis.

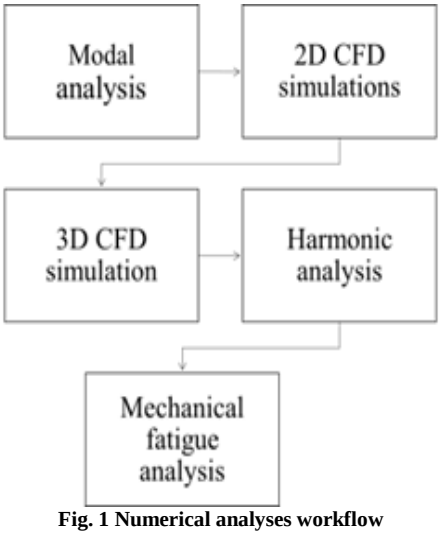

Fig. 1 Numerical analyses workflow

3.1. VWT Geometry and Material Properties

The studied model is a scale model proposed by Cajas consisting of components: a rigid conical mast and a flexible mounting structure of circular cross-section, as shown in Figure 2 [25]. The model is fixed as a cantilever beam, and its properties are detailed in Table 1.

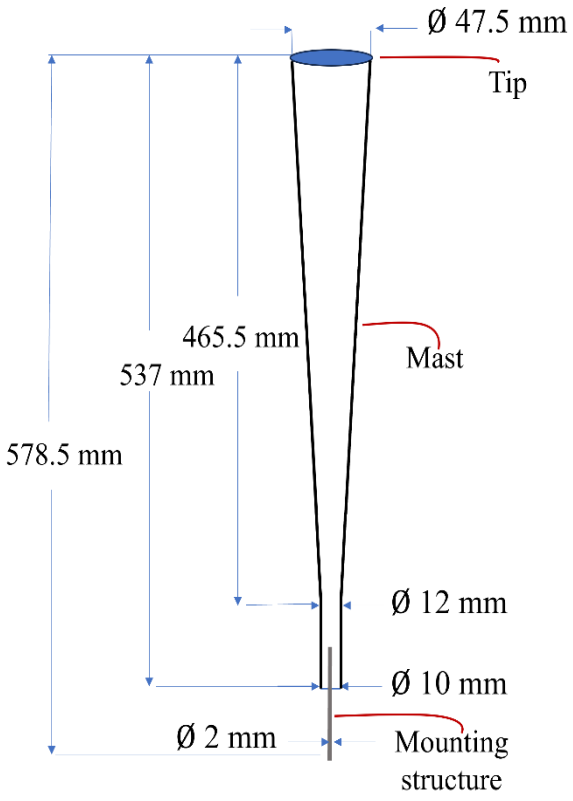

Fig. 2 Vortex wind turbine dimensions

Table 1. Properties of the VWT model

Element	Density (kg/m^3)	Young's Module (GPa)
Mast	246.9	300
Mounting structure	1365	97

3.2. Natural Frequency

The natural frequency value of the VWT allows estimating the resonance velocity using Equations (1) and (2). The modal analysis was performed using the Finite Element Method (FEM) in Ansys Modal, where the model was treated as an assembly with defined contact between the elements. A fixed boundary condition was applied at the base of the mounting structure, and the material properties used in the analysis are provided in Table 1. The FEM model was discretized using an unstructured mesh, as shown in Figure 3. The mesh convergence analysis was carried out based on mesh density parameters; for this purpose, four unstructured meshes with different maximum element sizes were made. To ensure mesh independence in numerical simulations, a Grid Convergence Index (GCI) analysis was conducted. This study aims to determine the most efficient mesh that provides accurate results with minimal computational cost.

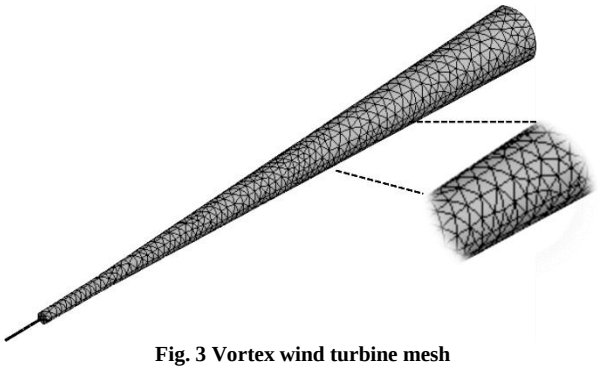

Fig. 3 Vortex wind turbine mesh

Table 2 shows the results of the mesh convergence analysis using the computed natural frequency as a parameter. Mesh 2-4 computes with greater accuracy the experimental first natural frequency value reported by Cajas, with an error margin of less than 4% [25].

Table 2. FEM mesh convergence results

	Model	Elements number	First natural frequency (Hz)
Cajas [25]	Experimental	--	5.3
	Numeric	--	4.8
Present	Mesh 1	8 158	5.70
	Mesh2	27 362	5.47
	Mesh3	52 012	5.46
	Mesh 4	119 426	5.47

Moreover, the results in Table 3 indicate that Mesh 2 presents a balance between precision and computational efficiency. Further refinement beyond this does not significantly affect the results, confirming mesh independence.

Table 3. GCI for different FEM mesh sizes

Mesh Pair	Frequency Difference	GCI (%)
Mesh 1-2	0.23	4.2
Mesh 2-3	0.01	0.18
Mesh 3-4	0.01	0.18

3.3. Resonance Velocity and Re-St Relation

The velocity range at which the turbine approaches resonance was estimated using Equation 3 and the experimental Re-St curve reported by Goldstein [22]. The vortex shedding frequency (f) was assumed to match the first natural frequency of the VWT, while d corresponds to the maximum diameter of the turbine's geometry. The Strouhal number (St) was considered within the range of 0.17–0.21, as

this interval accounts for the possible variations due to the flow characteristics and the geometry of the turbine. This range reflects the realistic extremes of *St*, ensuring that the resonance conditions are accurately captured within the experimental setup.

$$u = \frac{fd}{St} \quad (3)$$

The analysis suggests that the resonance velocity ranges between 1 and 1.5 m/s. Additionally, the velocities listed in Table 4 were analyzed to validate the numerical model over a broader range of *Re*. The working fluid is air at standard conditions, and its properties are 1.7894 x 10^{-5} (kg/ms) and density=1.225kg/m^3.

Table 4. Inlet boundary conditions for 2D CFD simulation

Velocity (m/s)	Re for 0.0475 m diameter
0.1	$2.65x10^2$
0.5	$1.33x10^3$
1.0	$2.65x10^3$
1.1	$2.91x10^3$
1.2	$3.18x10^3$
1.3	$3.45x10^3$
1.4	$3.71x10^3$
1.5	$3.98x10^3$
2.0	$5.31x10^3$
2.5	$6.64x10^3$

To determine the Reynolds-Strouhal relationship for this case study, 2D CFD computations in Ansys Fluent were performed under the conditions described earlier. The k-ω turbulence model was employed to resolve the vortex wake, following the approach of [12, 14]. A convergence criterion of $1x10^{-6}$ was set. The total time of simulation was 30 seconds, with a time step of 0.0125 s. The 2D domain was defined at the normal plane located at height h, at the highest part of the wind turbine, as illustrated in Figure 4.

The 2D meshing was carried out with hexahedral elements; three meshes with different densities were made. To perform the sensitivity analysis of the mesh, transient simulations (for a wind condition) were carried out; this analysis was performed based on the vortex detachment frequency. The analysis revealed that the results were independent of mesh density. Consequently, mesh 2 was selected for further use. The results of this analysis are presented in Tables 5 and 6.

Table 5. Mesh convergence results for 2D CFD

Mesh	Elements number	Vortex detachment frequency (Hz)
1	29,869	5.4725
2	63,548	5.4724
3	165,664	5.4724

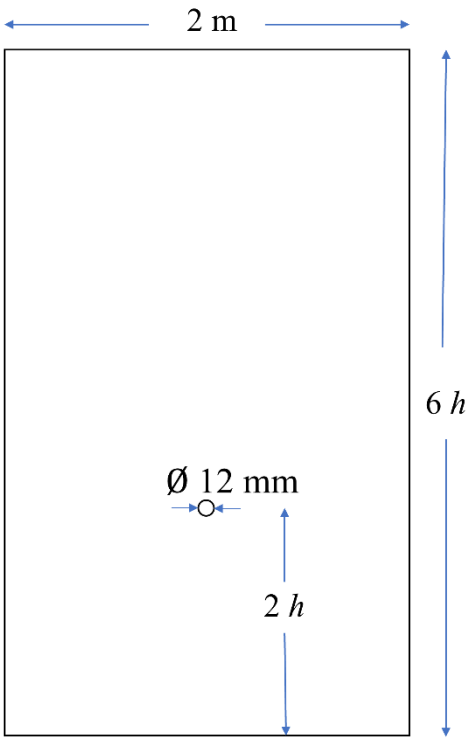

Fig. 4 2D domain to determine the Reynolds-Strouhal relationship at the tip of VWT

Table 6. Grid Convergence Index for 2D CFD

Mesh pair	Vortex detachment frequency difference	GCI (%)
Mesh 1-2	0.0001	0.001
Mesh 2-3	0.0000	0.000

3.4. Harmonic Analysis and Fatigue Life

To conduct the harmonic and fatigue life analysis, a 3D CFD model was first created using the resonance velocity obtained from the 2D CFD simulations. The total pressure profile derived from the 3D CFD model serves as the input condition for calculating oscillations in the VWT. The 3D CFD simulations were performed in a steady-state, utilizing the k-ω turbulence model in Ansys Fluent. The inlet velocity profile varied with height, reflecting the roughness of the surface ground, thereby emulating the behavior of the atmospheric boundary layer and ensuring a constant vortex detachment frequency over the height (*h*). The velocity profile was calculated using Equations (4) and (5), and the developed profile is illustrated in Figure 5.

$$u = \frac{u^*}{\kappa} ln\left(\frac{z+z_0}{z_0}\right) \quad (4)$$

Where u^* is the friction velocity, κ is the Von Karman constant= 0.41, z is the position in h, and z_0 is the aerodynamic roughness length. Friction velocity is defined as follows:

$$u^* = \frac{u_{ref}\kappa}{ln\left(\frac{z_{ref}+z_0}{z_0}\right)} \quad (5)$$

Where $u_{ref} = 1.5\ m/s$ is the reference means streamwise wind speed at z_{ref} , and $z_{ref} = 0.5785\ m$ is the reference height.

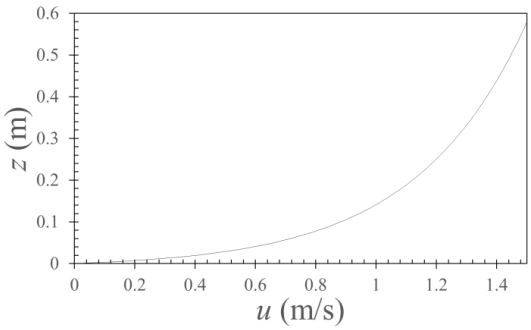

Fig. 5 Inlet velocity profile for 3D CFD

The 3D domain geometry was determined based on height (*h*), as shown in Figure 6. The 3D CFD mesh was formed with tetrahedral elements and a refinement in the area near the wind turbine. For the mesh sensitivity analysis, four meshes with different densities were generated, and the velocity values at the right lateral point of the VWT were compared. Table 7 presents the velocity comparisons for each mesh configuration. For this case, mesh 3 presents a balance between precision and computational efficiency, because in accordance with Table 8, the Grid Convergence Index (GCI) is less than 1.

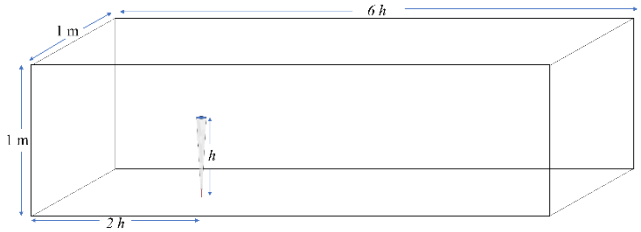

Fig. 6 3D CFD geometry

Table 7. Mesh convergence results for 3D CFD

Mesh	Elements Number	Velocity (m/s)
1	2,364,163	2.0210
2	3,703,765	1.9158
3	4,148,194	1.8985
4	5,463,017	1.8986

Table 8. Grid convergence Index for the 3D CFD

Mesh Pair	Frequency Difference	GCI (%)
Mesh 1-2	0.0521	5.491
Mesh 2-3	0.0090	0.911
Mesh 3-4	0.0001	0.005

The maximum displacements and bending angles of the VWT under resonant conditions were determined using harmonic analysis in Ansys. The input condition was the total pressure profile obtained from the 3D CFD simulation. The frequency range studied was 0 to 10 Hz, with the same physical constraints as those of the modal analysis; damping effects were not considered.

Besides evaluating the VWT's fatigue life, a mechanical fatigue analysis was conducted at the same frequencies as the harmonic analysis. The VWT comprises two main components: the mast and the mounting structure, with the latter being subjected to cyclic dynamic bending loads. For the fatigue analysis, the mounting structure was modeled as a cantilever beam under a bending force at its free end. This bending force was calculated using Equations (6) and (8) and is depicted in the schematic shown in Figure 7.

$$F = \frac{2\theta EI}{L^2} \quad (6)$$

Where θ is the bending angle, E is the Young´s modulus, I is the inertia moment, and L is the mounting structure height.

$$I = \frac{\pi \phi^4}{64} \quad (7)$$

Where ø is the mounting structure height diameter.

$$\theta = sin^{-1}\frac{M}{h} \quad (8)$$

Where M is the maximum displacement.

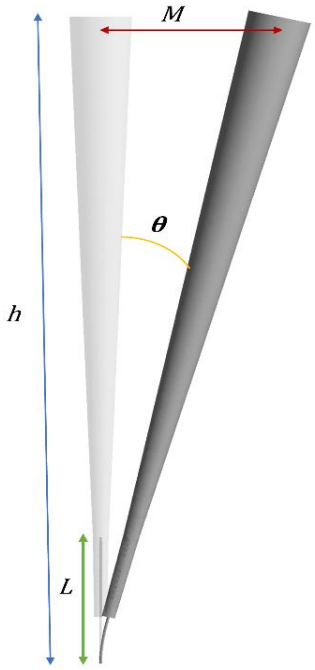

Fig. 7 Bending angle to compute the bending force used in the harmonic analysis

The mechanical and fatigue characteristics of the mounting structure were not specified by Cajas [25]. However, Peksen reports that these types of wind turbines are manufactured using carbon fibers and polymers reinforced with carbon or glass fibers [32]. For the analysis, the mechanical properties of a carbon fiber composite with density and Young's modulus similar to those reported by Cajas were used [25]. Table 9 shows the comparison of the mechanical properties reported by Cajas against those of the proposed material [33].

Table 9. Material properties comparison

Physical Properties	Cajas [25]	Epoxy/Carbon Fiber Composite 77904 [35]
Density (kg/m$^{3)}$	1365	1400
Young's modulus (GPa)	97	96.9
Tensile Strength, Ultimate (MPa)	---	878
Tensile Strength, Yield (MPa)	---	1230
Compressive Yield Strength (MPa)	---	725

The fatigue study is based on a stress-lifetime analysis, so the S-N curve of a carbon fiber composite obtained experimentally by [34] is used; the adopted S-N curve is derived and fitted by the following function:

$$ln\,N = \frac{1943.6 - S}{44.93} \quad (9)$$

Where S is the stress in the mounting structure.

4. Results

The results obtained in this work provide an understanding of the vortex wind turbine's dynamic behavior. By coupling CFD-FEM models, it was possible to reproduce the fluid-structure interaction in a more realistic manner, identifying the effects of resonance on the deformations, stresses, and service life of the structure.

Compared to previous results [31], which use simplified models, this work integrates aerodynamic and structural analysis for a wide range of Reynolds numbers, seeking to reproduce the real phenomenon at each step, thus reducing simplifications.

The numerical model was validated by comparing the turbine displacement amplitudes and the Re-St ratio with the experimental results reported by Cajas and Goldstein, respectively, showing agreement with both studies. The details of these comparisons are presented in sections 4.1 -4.2. [22, 25].

4.1. Resonance Velocity and Re-St Relation

The results presented in Table 10 indicate that the resonance velocity is 1.5 m/s. This velocity causes the vortex shedding frequency to match the first natural frequency of the VWT. Additionally, the vortex shedding frequency is directly related to the Reynolds number (*Re*); as *Re* increases, the frequency also increases.

The *Re-St* relationship in Figure 8, derived from Table 10, shows good agreement with the experimental curve reported by Goldstein, with an approximate deviation of 3.8% [22]. This minimal discrepancy indicates that the theoretical results offer an accurate representation of the experimentally observed behavior. The differences between the experimental and numerical models can be attributed to simplifications of the mathematical model used in the numerical model, to the flow transition regime, and to the sensitivity of the Strouhal number to small variations in experimental conditions.

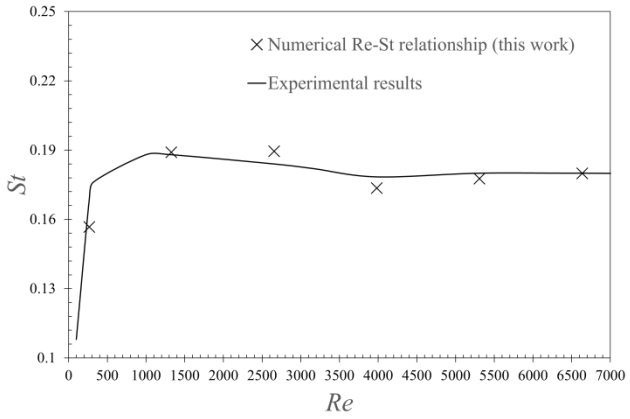

Fig. 8 Numerical Re-St relationship vs. experimental results [22]

Table 10. 2D CFD results summary

Velocity (m/s)	*Re*	Vortex Shedding Frequency (Hz)
0.1	2.65x10^2	0.33
0.5	1.33x10^3	1.99
1.0	2.65x10^3	3.99
1.1	2.91x10^3	4.3
1.2	3.18x10^3	4.5
1.3	3.45x10^3	4.8
1.4	3.71x10^3	5.1
1.5	3.98x10^3	5.48
2.0	5.31x10^3	7.48
2.5	6.64x10^3	9.47

4.2. Harmonic Analysis and Fatigue Life

Figure 9 shows the vortices behind the VWT at different turbine heights using streamlines. The image is divided into eight sections, each representing the flow at different turbine heights, ranging from 98.5% to 12.5% *h*, where *h* represents

the total height of the VWT. These sections show the variation in vortex shedding along the cylinder. Vortex spacing and length are observed to change with height: At higher heights (98.5% - 75% *h*), the vortices are larger and more unstable, showing strong interaction with the surrounding flow.

- At intermediate heights (62.5% - 50% *h*): The vortices are well-defined and elongated, indicating a strong contribution to energy generation.
- At lower heights (37.5% - 12.5% *h*), the vortices become smaller and less intense, suggesting a lower aerodynamic contribution in these regions.

Additionally, it can be observed that the vortex length reaches its maximum around 75% of the total height, extending up to 3 times the cylinder diameter. This indicates that this zone is important for vortex formation and shedding.

Finally, it is observed that boundary layer shedding occurs around 90° and 270° with respect to the flow direction, indicating that the flow separates just after the maximum curvature of the cylinder. The value of this angle depends on the interaction between the boundary layer and the geometry, as well as the Reynolds number (*Re*), surface roughness, and flow conditions.

The analyzed flow is a transitional flow that allows for symmetric separation and stable periodic oscillations. This enables synchronization between the vortex shedding frequency and the natural frequency of the VWT, a key aspect for wind energy harvesting based on vortex-induced resonance.

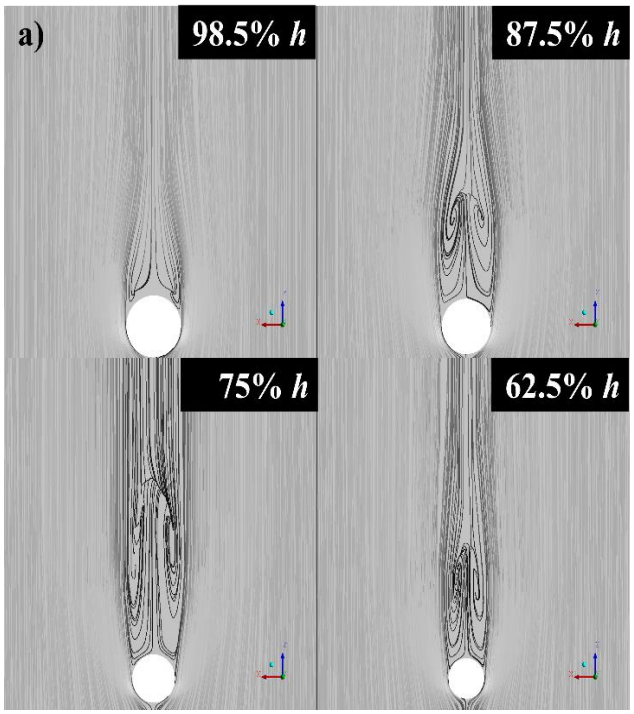

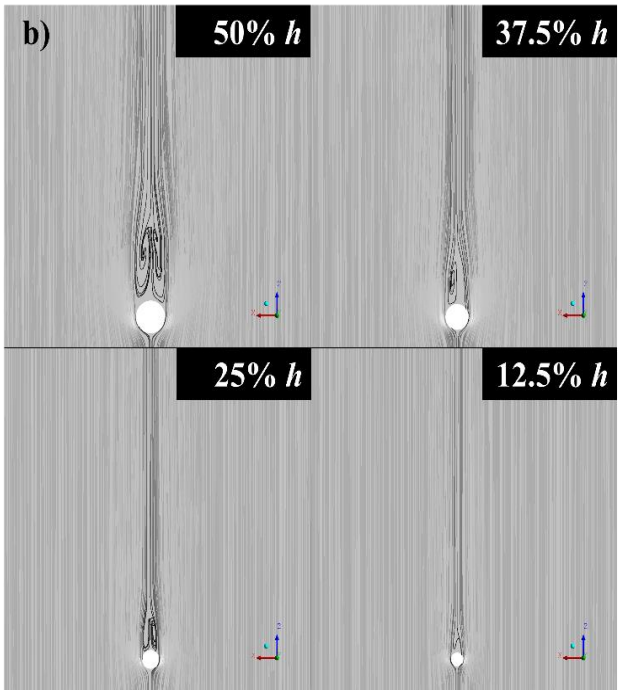

Fig. 9 Computed Vortex at different VWT heights, (a) 98.5 -62.5 % *h* zone, and (b) 50-12.5 % *h*.

The harmonic results are presented in Figure 10, where it can be seen that the VWT displacement amplitude depends directly on the excitation frequency. The closer the excitation frequency is to the resonant frequency, the greater the VWT displacement, reaching its peak at 5.48 Hz.

The maximum displacement amplitude observed is 17 mm and deviates by 0.4% and 5.6% from the experimental and numerical results reported by Cajas, respectively [25]. This maximum condition causes stress concentrations near the anchorage zone, indicating that this is the area most sensitive to wind-induced resonance.

Figure 10 shows the fatigue life results, where for frequencies lower than 5.3 Hz and higher than 5.7 Hz, the VWT life is infinite. This is because when the life in cycles reaches or exceeds $1x10^6$, the material enters a “fatigue limit” phase, where it can theoretically withstand an infinite number of cycles without failing [34].

Furthermore, in Figure 11, it is observed that the turbine can operate continuously at resonance (5.48 Hz) for up to 15 hours without failing due to cumulative damage. This is because the accumulated damage under this condition is less than 1; according to the Palmgren-Miner linear damage rule, failure does not occur when the accumulated damage does not reach this threshold [36]. However, after this period, cumulative damage will cause failure. For the rest of the operating frequencies analyzed, the turbine can operate continuously for 24 hours without failing.

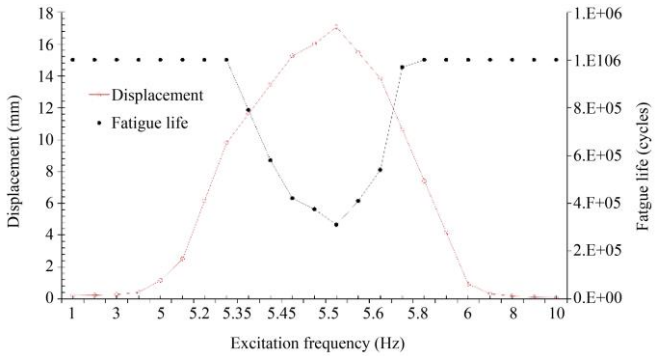

Fig. 10 Displacement amplitude from the harmonic response and fatigue life of VWT

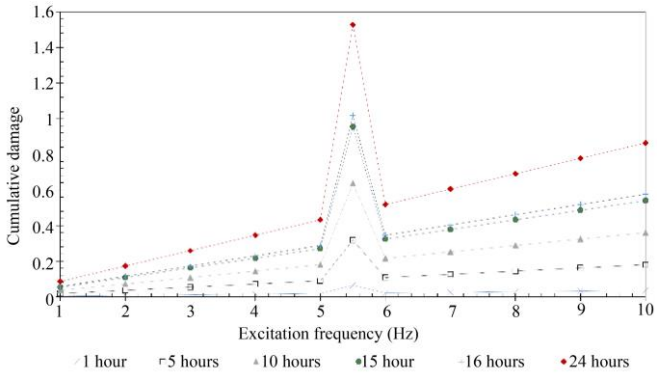

Fig. 11 Cumulative damage of VWT for different excitation frequencies

5. Conclusion

To induce wind resonance, the wind must produce alternating vortex shedding at a frequency close to the Vortex Wind Turbine's natural frequency. This can be accomplished by adjusting the flow properties or altering the turbine's dimensions. The objective of the turbine is to reach the resonance phenomenon to take full advantage of the maximum displacements generated during this state. However, these displacements subject the structure to intense stresses.

The results obtained allow us to conclude that the wind turbine can operate continuously outside the resonance range without the risk of failure due to mechanical fatigue, since the stresses generated for this condition are lower than the fatigue limit of the material. This allows us to conclude that the structure's service life exceeds the operational requirements and minimizes the risk of long-term fatigue failure. However, if it operates within the resonance range (5.31–5.69 Hz), continuous operation is safe for up to 15 hours before the risk of failure arises, since in this operating condition, materials may present fatigue stresses greater than their physical limits.

Therefore, the turbine can operate safely under resonance conditions, provided the established limits are respected. Otherwise, any variation in the properties of the materials or the system will directly alter the fatigue risk and the maximum calculated service life, which requires these limits to be applied with rigorous caution in the final design. The results presented allow for the establishment of design criteria that take advantage of the wind-induced resonance phenomenon without compromising the integrity of the structure.

Acknowledgments

The first author thanks SECIHTI for the scholar grants 966584.

References

[1] David Jesus Yañez Villarreal, "Vortex Resonance Wind Turbine," *European Patent EP2602483A1*, pp. 1-11, 2016. [Google Scholar] [Publisher Link]

[2] Elmar Achenbach, "Vortex Shedding from Spheres," *Journal of Fluid Mechanics*, vol. 62, no. 2, pp. 209-221, 1974. [CrossRef] [Google Scholar] [Publisher Link]

[3] Ali Ashouri et al., "Numerical Investigation on Two-Degree-of-Freedom Vortex-Induced Vibration of a Circular Cylinder in Power-Law Fluids," *Journal of Non-Newtonian Fluid Mechanics*, vol. 292, 2021. [CrossRef] [Google Scholar] [Publisher Link]

[4] Wei Wang, and Penghao Duan, "Vortex-Induced Vibration Response of the Cylinder Inspired by Terebridae," *Marine Structures*, vol. 94, 2024. [CrossRef] [Google Scholar] [Publisher Link]

[5] Hangzhao Liu et al., "Effects of a Splitter on the Vortex-Induced Vibration of a 5:1 Rectangular Cylinder," *Physics of Fluid*s, vol. 36, no. 1, 2024. [CrossRef] [Google Scholar] [Publisher Link]

[6] Abhishek Kumar, S.P. Das, and Shaligram Tiwari, "Wall Effect on the Wake Characteristics of a Transversely Rotating Sphere," *Physics of Fluids*, vol. 36, no. 1, 2024. [CrossRef] [Google Scholar] [Publisher Link]

[7] Weilin Chen et al., "Three-Dimensional Flow Past Two Stationary Side-by-Side Circular Cylinders," *Ocean Engineering*, vol. 244, 2022. [CrossRef] [Google Scholar] [Publisher Link]

[8] Hamid Rahman et al., "Aerodynamic Characteristics and Wake Formation Behind a Pair of Side-by-Side Rectangular Cylinders using the Lattice Boltzmann Method," *Ocean Engineering*, vol. 303, 2024. [CrossRef] [Google Scholar] [Publisher Link]

[9] Robert Muyshondt et al., "Experimental Measurements of the Wake of a Sphere at Subcritical Reynolds Numbers Free," *Journal of Fluids Engineering*, vol. 143, no. 6, pp. 1-19, 2021. [CrossRef] [Google Scholar] [Publisher Link]

[10] Jiang-Hua Li et al., "Vortex Dynamics and Boundary Layer Transition in Flow Around a Rectangular Cylinder with Different Aspect Ratios at Medium Reynolds Number," *Journal of Fluid Mechanics*, vol. 982, 2024. [CrossRef] [Google Scholar] [Publisher Link]

[11] Marek Jan Janocha et al., "Flow Around Two Elastically-Mounted Cylinders with Different Diameters in Tandem and Staggered Configurations in the Subcritical Reynolds Number Regime," *Marine Structures*, vol. 76, pp. 1-20, 2021. [CrossRef] [Google Scholar] [Publisher Link]

[12] Zhiyong Huang, Muk Chen Ong, and Carl Martin Larsen, "Wake Structures and Vortex-induced Forces of a Controlled In-line Vibrating Circular Cylinder," *Ocean Engineering*, vol. 189, pp. 1-12, 2019. [CrossRef] [Google Scholar] [Publisher Link]

[13] Rajesh Bhatt, and Md. Mahbub Alam, "Vibrations of a Square Cylinder Submerged in a Wake," *Journal of Fluid Mechanics*, vol. 853, pp. 301-332, 2018. [CrossRef] [Google Scholar] [Publisher Link]

[14] Hongyi Jiang, and Liang Cheng, "Strouhal-Reynolds Number Relationship for Flow Past a Circular Cylinder," *Journal of Fluid Mechanics*, vol. 832, pp. 170-188, 2017. [CrossRef] [Google Scholar] [Publisher Link]

[15] Yan Liu, Jun Liu, and Fu-Ping Gao, "Strouhal Number for Boundary Shear Flow Past a Circular Cylinder in the Subcritical Flow Regime," *Ocean Engineering*, vol. 269, pp. 1-13, 2023. [CrossRef] [Google Scholar] [Publisher Link]

[16] Javad Farrokhi Derakhshandeh, "Wake-Induced Vibration of an Elastic Plate Submerged in the Wake of Tandem Circular Cylinders," *Physics of Fluids*, vol. 36, no. 3, 2024. [CrossRef] [Google Scholar] [Publisher Link]

[17] Siva Ramalingam, Rong Fung Huang, and Ching Min Hsu, "Effect of Crossflow Oscillation Strouhal Number on Circular Cylinder Wake," *Physics of Fluids*, vol. 35, no. 9, 2023. [CrossRef] [Google Scholar] [Publisher Link]

[18] Yu Wang et al., "Dynamic Evolution of Strouhal Number in Flexible Pipes Coupling Rotation," *International Journal of Mechanical Sciences*, vol. 263, 2024. [CrossRef] [Google Scholar] [Publisher Link]

[19] Hassan el Sheshtawy et al., "Experimentally Investigated Vortex-Induced Vibration of a High Aspect Ratio and Small Mass Ratio Circular Cylinder Oscillating in Low Reduced Velocity Flows," *Ocean Engineering*, vol. 238, 2021. [CrossRef] [Google Scholar] [Publisher Link]

[20] J.F. Derakhshandeh, and M.M. Alam, "A Review of Bluff Body Wakes," *Ocean Engineering*, vol. 182, pp. 475-488, 2019. [CrossRef] [Google Scholar] [Publisher Link]

[21] Tomas Martinez Piquer, "*Velocity Measurement by Vortex Shedding. Contribution to the Measurement of Mass Flow Rates.*," Doctoral Thesis, Polytechnic University of Madrid, pp. 1-243, 1988. [Google Scholar] [Publisher Link]

[22] Sydney Goldstein, *Modern Developments in Fluid Dynamics; an Account of Theory and Experiment Relating to Boundary Layers, Turbulent Motion and Wakes*, Clarendon Press, vol. 2, pp. 1-702, 1938. [Google Scholar] [Publisher Link]

[23] H. Sakamoto, and H. Haniu, "A Study on Vortex Shedding From Spheres in a Uniform Flow," *ASME Journal of Fluids Engineering*, vol. 112, no. 4, pp. 386-392, pp. 1-7, 1990. [CrossRef] [Google Scholar] [Publisher Link]

[24] A. Chizfahm, E. Azadi Yazdi, and M. Eghtesad, "Dynamic Modeling of Vortex Induced Vibration Wind Turbines," *Renewable Energy*, vol. 121, pp. 632-643, 2018. [CrossRef] [Google Scholar] [Publisher Link]

[25] Juan Carlos Cajas García et al., "*SHAPE Project Vortex Bladeless: Parallel Multi-Code Coupling for Fluid-Structure Interaction in Wind Energy Generation*," Partnership for Advanced Computing in Europe: PRACE 4th Implementation Phase Project (EC-H2020-653838), Research Report, pp. 1-6, 2016. [Google Scholar] [Publisher Link]

[26] A.H. Techet, F.S. Hover, and M.S. Triantafyllou, "Vortical Patterns behind a Tapered Cylinder Oscillating Transversely," *Journal of Fluid Mechanics*, vol. 363, pp. 79-96, 1998. [CrossRef] [Google Scholar] [Publisher Link]

[27] Sigil Francis, V. Umesh, and S. Shivakumar, "Design and Analysis of Vortex Bladeless Wind Turbine," *Materials Today: Proceedings*, vol. 47, pp. 5584-5588, 2021. [CrossRef] [Google Scholar] [Publisher Link]

[28] Miguel Ángel Sánchez Hidalgo, Ricardo Atienza Pascual, and David Yáñez Villarea, "Design and Optimization of a Cylindrical Geometric Structure for Uniform Detachment of Von Karman Vortices," *Technology and Development*, vol. 15, pp. 1-23, 2017. [Google Scholar] [Publisher Link]

[29] R.C. Hibbeler, *Mechanics of Materials*, Pearson, pp. 1-896, 2018. [Google Scholar] [Publisher Link]

[30] David Jesús Yáñez Villarreal, "*Aerogeneradores Resonantes Por VIV*," Vortex Bladeless, pp. 1-6, 2018. [Google Scholar] [Publisher Link]

[31] Janis Breen, and Wrik Mallik, and Sondipon Adhikari, "Performance Analysis and Geometric Optimization of Bladeless Wind Turbines using Wake Oscillator Model," *Renewable Energy*, vol. 254, pp. 1-10, 2025. [CrossRef] [Google Scholar] [Publisher Link]

[32] Murat Peksen, *Multiphysics Modelling: Materials, Components, and Systems*, Academic Press, pp. 1-282, 2018. [Google Scholar] [Publisher Link]

[33] Overview of Materials for Epoxy/Carbon Fiber Composite, MatWeb Material Property Data. [Online]. Available: https://www.matweb.com/search/datasheettext.aspx?matguid=39e40851fc164b6c9bda29d798bf3726

[34] F. Delmotte, "*Fatigue Characterization of Unidirectional Carbon Fiber Composites at 0 and 15*," Universidad of Sevilla, Technical Report, 2013. [Google Scholar]

[35] Richard Gordon Budynas, and J. Keith Nisbett, *Shigley's Mechanical Engineering Design*, 11th ed., McGraw-Hill Education, pp. 1-1095, 2020. [Google Scholar] [Publisher Link]

[36] Milton A. Miner, "Cumulative Damage in Fatigue," *Journal of Applied Mechanics*, vol. 12, no. 3, pp. 159-164, 1945. [CrossRef] [Google Scholar] [Publisher Link]